PHYSICAL PROPERTIES OF ONSAGER'S DIPOLE CHAIN MODEL FOR IONIC TRANSPORT ACROSS MEMBRANES

I. STEADY-STATE FLUXES AND INSTABILITIES

J. SCHNAKENBERG

From the Battelle-Institut e.V., Frankfurt am Main, West Germany. Dr. Schnakenberg's present address is the Institut für Theoretische Physik, Rheinisch-Westfälische Technische Hochschule, 51 Aachen, Templergraben 64, West Germany.

ABSTRACT The steady-state fluxes in Onsager's model for ionic transport along a dipole chain are derived by application of Hill's diagrammatic technique for unimolecular systems. It is shown that under specific conditions the chain exhibits thermodynamic instabilities which prove to be a possible explanation for the phenomenon of electrical excitation in biological membranes.

1. INTRODUCTION

Fixed facilities for ionic transport across biological membranes are usually described as pores or channels which are formed by helical protein structures. In order to account for the high selectivity of ionic transport across membranes, one has to assume that these pores are very narrow (of the order of the ionic diameter). The ions will pass the pores in single-file motion, the unit step of transport being a hopping transition between two stable sites in the pore.

Up to now, both light and electron microscopy have failed to give clear evidence of the structural details of the pore model: narrow protein helices providing a pathway of stable sites for ions. Moreover, the essential physical features of ionic transport across biological membranes may equally well be explained on the basis of models with only a few structural assumptions. A strikingly simple but very convincing model has recently been proposed by Onsager (1): ionic transport along a chain of elementary molecular dipoles. Such a chain could be formed by a single extended protein molecule, and possible candidates for the elementary molecular dipoles are hydroxyl and carboxyl groups in the side chains of amino acids.

This dipole chain has two low energy configurations: all positive ends are directed towards the outside or inside (left or right side of the membrane). Clearly, an ap-

plied electric field causes an energy difference between these configurations proportional to the field.

Let the dipole chain be in its low energy configuration with all positive ends inside (right-hand side). A cation from the outside, say of type 1, can now cross the membrane along the chain by adjoining the negative end of the innermost dipole, jumping over it, and simultaneously reversing its direction and so forth, until it arrives at the inner (right-hand) side of the membrane. After having passed the chain, the ion has reversed the chain's polarization compared with that at the beginning. Thus, no further ion of type 1 can pass the same chain in the same direction, and a steady ionic flux of type 1 will not be sustained unless the chain is capable of rearranging itself appropriately to the original polarization. Such a rearrangement could be accomplished by (*a*) passage of an anion (type 2) in the same direction as cation 1, (*b*) passage of a cation (type 2) in the opposite direction, (*c*) passage of a directional discontinuity or "bonding defect" of the ordered chain in any of the two possible directions.

In the latter case, there is a net flux of electric charge, and the ionic flux is controlled by an applied field. This also holds for cases *a* and *b* if the absolute values of the valencies of ions 1 and 2 are different.

From the physical point of view, Onsager's model provides a mechanism for screening the ionic charge against the hydrophobic interior of the membrane. While an ion of charge $\nu_1 e$ (e is the elementary charge, ν_1 the valency) traverses the dipole chain from left to right, the actually transferred charge is $\nu_1 e - 2q$ (q is the effective amount of charge at the ends of the elementary dipoles) rather than $\nu_1 e$. If the chain is rearranged by the passage of a cation of charge $\nu_2 e$ from right to left or of a bonding defect in any direction, the actual charge transfer in the second step is $-\nu_2 e + 2q$ or $2q$.

In this paper we are going to study the essential physical properties of the model in steady state: ionic and electric fluxes as a function of the voltage and the ionic concentrations. Time-dependent phenomena such as chain vibrations and relaxation will be investigated in part II of this paper.

In section 2 of this part, the physical features of the model and its essential parameters are briefly described. In section 3, the steady-state fluxes as functions of the voltage and concentrations are derived for versions 2 and 3 of the model, namely for antiparallel transit of two cations and transit of one cation and two types of bonding defects. This derivation is based on Hill's (2) diagram technique for steady-state fluxes of unimolecular systems. Although the results are algebraically not very simple, numerous qualitative conclusions will be drawn in section 4 by straightforward arguments which pertain in particular to the asymptotic behavior for voltage $U \rightarrow \infty$ and the occurrence of instabilities. A possible relationship between such instabilities and the phenomenon of electrical excitation in biological membranes is discussed. A numerical evaluation of the results of section 3 is presented in section 5.

2. DESCRIPTION OF THE MODEL

Let us consider a linear chain of n equal molecular dipoles each of which has the dipole moment p. For the sake of simplicity we assume that the chain is precisely straight-lined and that its direction is perpendicular to the membrane surfaces. We could generalize the following calculations to include slightly curved chains, but we do not expect that the results would be significantly altered in this way.

The dipole chain touches the membrane surfaces at both ends. If D denotes the membrane thickness, we can define $a = D/n$ as the lattice constant of our one-dimensional system. Clearly, we have $a \geq l$, where l is the length of a single molecular dipole.

Let us further assume that each dipole is capable of rotating about its center. This rotation is either completely free (the dipole ends moving on a sphere), or else the dipoles rotate about a fixed axis (the ends moving on a circle). Because of the electrostatic interaction between adjacent dipoles, the chain configurations with minimum potential energy are those where all dipoles are uniformly directed parallel to the chain:

$$\rightarrow\rightarrow\rightarrow \ldots \rightarrow, \tag{1a}$$

$$\leftarrow\leftarrow\leftarrow \ldots \leftarrow. \tag{1b}$$

If an electric field F is applied ($F > 0$ from left to right), we have

$$E_b - E_a = npF, \tag{2}$$

where E_b and E_a are the potential energies of configurations b and a in Eqs. 1.

The lowest dynamic excitations of the configurations a and b are chain vibrations very similar to phonons in solids. During these vibrations each dipole performs small rotational oscillations abound its center. Because of the dipole-dipole interactions, there is a frequency- or wave-vector-dependent phase correlation between adjacent dipoles. We shall discuss the chain vibrations in detail in part II of this paper.

Let us now consider dynamically stable chain configurations different from those in Eqs. 1 and thus involving higher potential energies. Clearly, each directional discontinuity or bonding defect along the chain increases the potential energy by an amount w. Configurations with energy w ($E_b = E_a = 0$ for $F = 0$) include:

$$\rightarrow\rightarrow \ldots \rightarrow\leftarrow \ldots \leftarrow, \tag{3a}$$

or

$$\leftarrow\leftarrow \ldots \leftarrow\rightarrow \ldots \rightarrow, \tag{3b}$$

and those with energy $2w$

$$\rightarrow \ldots \rightarrow\leftarrow \ldots \leftarrow\rightarrow \ldots \rightarrow, \tag{4}$$

or

$$\leftarrow \ldots \longleftrightarrow \ldots \rightarrow\!\leftarrow \ldots \leftarrow,$$

and so forth.

Let us estimate the order of magnitude of w. If we have, for example, extended dipoles $l \lesssim a$ spaced at small intervals $s = a - l \ll a$ and the electric charge q localized at the ends of the dipoles as indicated in Fig. 1 *a*, the electrostatic interaction between adjacent dipoles is mainly due to the electrostatic attraction or repulsion of the next-neighboring charges $\pm q$.

In this case, with $p = q \cdot l$, we find

$$w \approx 2\frac{q^2}{s} = 2\frac{p^2}{l^2 s} = 2\frac{\alpha^2 e^2}{s}\left(\frac{a}{l}\right)^2 \approx 2\frac{\alpha^2 e^2}{s}, \tag{5}$$

where we have introduced the notation

$$\alpha = \frac{p}{ea}, \tag{6}$$

$\alpha = 1$ denoting dipoles of maximum length with elementary charges e at their ends. For a realistic estimate we assume $0.1 \leq \alpha \leq 0.2$ and $2\ \text{Å} \leq s \leq 4\ \text{Å}$. This yields a w value between 0.1 and 0.5 eV. The thermodynamic Boltzmann factor $\exp(-w/k_B T)$ for the configuration with exactly one-directional discontinuity (at $T = 300°\text{K}$) would then be of the order of 10^{-2}–10^{-9}, the actual value depending sensitively on the precise value of w.

In the case of long distances $s \lesssim a$ and short dipoles $l \ll a$ (Fig. 1 *b*) the electrostatic interaction between adjacent dipoles is given by $-2p^2/s^3$, so that

$$w \approx 4\frac{p^2}{s^3} = 4\frac{\alpha^2 e^2}{s}\left(\frac{a}{s}\right)^2 \approx 4\frac{\alpha^2 e^2}{s}. \tag{7}$$

Comparing Eq. 7 with Eq. 5, we expect the same order of magnitude for w and $\exp(-w/k_B T)$ as in the case of short intervals.

The model we have described so far is, apart from the phonon-like vibrations of the chain, a one-dimensional finite Ising model. Unfortunately, the well-known results of the one-dimensional Ising model do not help us any further for biophysical applications. Firstly, the biophysical interest in our model is based on the possible presence of ions in the chain and the chain as a transport facility. These phe-

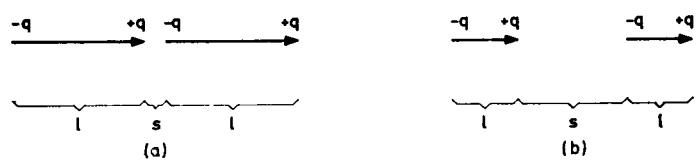

FIGURE 1 Electrostatic interaction at small (*a*) and large (*b*) intervals.

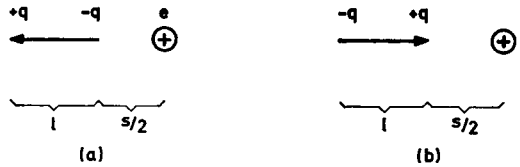

FIGURE 2 Polar environment of an ion in the dipole chain.

nomena are not included in the usual Ising model theory. Secondly, the usual theory of the Ising model is confined to the thermodynamic equilibrium, whereas in our case we shall see that also extreme nonequilibrium states are of interest. Finally, the Ising model only yields useful analytical results either for an infinite model or for $F = 0$. In our case, however, the number of dipoles will be of the order of 10, so that the theory of infinite models cannot be applied, and the case $F = 0$ is irrelevant.

Let us now extend our model to include the presence of ions in the chain. An ion will tend to polarize its surroundings. Then, the configuration with minimum potential energy becomes

$$\leftarrow \ldots \leftarrow\leftarrow \oplus \rightarrow\rightarrow \ldots \rightarrow. \tag{8}$$

Let us estimate the increase u in potential energy associated with a partial removal of the local polarization, i.e., the energy difference between the local configurations a and b as shown in Fig. 2. In the case of extended dipoles at short distances, configuration a of Fig. 2 exhibits an attraction energy of $2\ eq/s$, so that

$$u = 4\frac{eq}{s} = 4\frac{ep}{ls} = 4\frac{\alpha e^2}{s}\frac{a}{l} \approx 4\frac{\alpha e^2}{s}. \tag{9}$$

Insertion of $\alpha = 0.1$, $s = 4$ Å leads to $u \approx 1.4$ eV so that configuration b in Fig. 2 is thermodynamically very unlikely.

The same argument applies to the case of short dipoles at long distances where we have

$$u \approx 8\frac{ep}{s^2} = 8\frac{\alpha e^2}{s}\frac{a}{s} \approx 8\frac{\alpha e^2}{s}. \tag{10}$$

Next, we have to formulate the description of ionic transport in terms of reaction kinetics. The basic transport process consists of an ionic transition from one dipole interstice to a neighboring one. Simultaneously, the traversed dipole reverses its direction. We assume the rate constant of this process (without field) to be k_i, where i denotes the ionic species. If an electric field F is applied, the above process is associated with an electrostatic energy difference

$$\Delta\epsilon = \mp\left(\nu_i e\frac{D}{n} - 2p\right)F, \tag{11}$$

the sign depending on the direction of the process and $\nu_i e$ being the ionic charge. Half of this energy has to be thermally activated so that the transition rates for the two directions become

$$\mathbf{k}_i^{(\rightarrow)} = k_i e^{x_i}, \qquad \mathbf{k}_i^{(\leftarrow)} = k_i e^{-x_i},$$

$$x_i = (\nu_i - 2\alpha)\frac{eU}{2nk_B T}, \qquad U = F \cdot D, \tag{12}$$

where α is defined by Eq 6 and a positive voltage $U > 0$ corresponds to a field $F > 0$ from left to right (e is the elementary charge, T is the absolute temperature, k_B is the Boltzmann constant).

For processes where the ion enters the chain from the external electrolyte, we have to multiply the rate constants in Eq. 12 by the corresponding effective ionic concentrations c_i, c_i'. It should be pointed out that c_i and c_i' are not necessarily the absolute ionic concentrations in the electrolytes, but will contain a factor $\exp(-\epsilon/kT)$, where ϵ describes the difference between the ionic solvation energies in the electrolyte and in the dipole chain.

3. DERIVATION OF STEADY-STATE FLUXES

a. Two-Channel Model

Let us start our investigation of the steady-state properties of the model by looking at the case where two kinds of cations 1 and 2 can pass the dipole chain. In order to get a field-dependent flux of ions, we assume that the two kinds of ions have different valencies ν_1 and ν_2, for example $\nu_1 = 2$ (Ca^{2+}, Mg^{2+}) and $\nu_2 = 1$ ($Na+$, K^+, H^+).

By $A_k(B_k)$ we denote the states of the dipole chain with one ion of type 1 (or 2) in the interstice between dipoles k and $k+1$ and with complete directional ordering as indicated in Fig. 3. Clearly, $1 \leq k \leq n-1$, where n is the number of dipoles. R and L denote the states of the empty chain with complete polarization of the dipoles to the right and to the left, respectively (cases a and b in Eq. 1).

If $E(A_k)$, $E(B_k)$, $E(R)$, $E(L)$ denote the electrostatic energies of the chain in the states A_k, B_k, R, L (without field), we may write

$$\left.\begin{aligned} E(A_k) - E(L) = E(A_k) - E(R) = \epsilon_{DC}^{(1)} - \epsilon_s^{(1)} = \epsilon_1 > 0 \\ E(B_k) - E(L) = E(B_k) - E(R) = \epsilon_{DC}^{(2)} - \epsilon_s^{(2)} = \epsilon_2 > 0 \end{aligned}\right\}, \tag{13}$$

where $\epsilon_{DC}^{(i)}$ and $\epsilon_s^{(i)}$ are the solvation energies of the ion of type i in the chain and in the aqueous solution, respectively. All possible states of the chain not included in A_k, B_k, R, L would energetically be separated from R, L by at least the energy w

FIGURE 3 Definition of the state A_k.

of a bonding defect. By assuming

$$w \gg \epsilon_i, \quad i = 1, 2, \tag{14}$$

for the case presently under study, we may neglect all the states not included in A_k, B_k, R, L.

The states A_k. B_k, R, L can be represented in a diagram

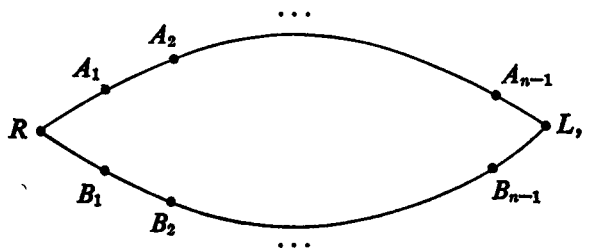

(15)

where each line connecting two states denotes an allowed transition between the states in either direction and thus carries two transition rates as given in Eq. 12. We have, for example,

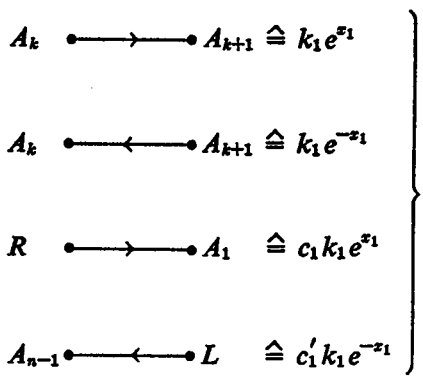

(16)

which applies analogously to type 2 ions.

The use of diagrams of the type shown in Eq. 15 is a rather general technique for treating first-order chemical reaction kinetics. The steady-state properties of such systems are most easily obtained by making use of the Kirchhoff theorem (3), rediscovered by Bott and Mayberry (4), King and Altmann (5), and Hill (2). According to this theorem, the steady-state flux along a particular line is given by the ratio of the sum of all flux diagrams along this line and the sum of all directed partial diagrams. A partial diagram is obtained from the original diagram in Eq. 15 by omitting the minimum possible number of lines such that the resulting diagram no longer contains any cycle (closed loop). From this partial diagram we construct a directed partial diagram by orienting all lines towards one single point of the diagram. The algebraic value of a directed partial diagram is the product of

the rate constants corresponding to the directed lines. The sum of all directed partial diagrams is a twofold summation over all ways of forming partial diagrams and over all possibilities of directing each of the undirected partial diagrams. From the original diagram of Eq. 15 this sum can be derived as follows:

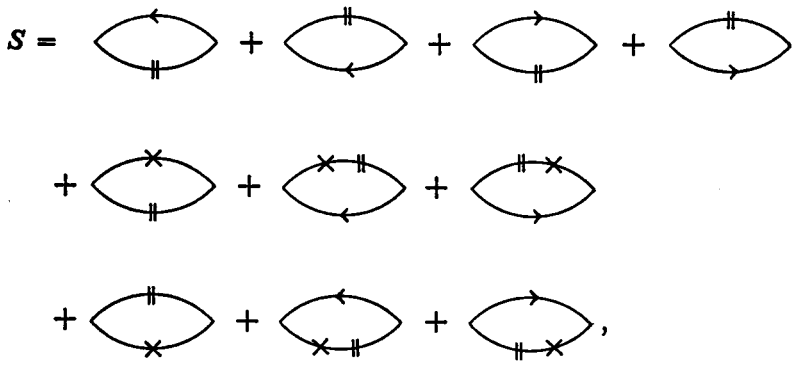

(17)

where, as in Eq. 15, the upper branch contains the transition rates of ion type 1 and the lower branch that of ion type 2. The following graphical abbreviations have been used:

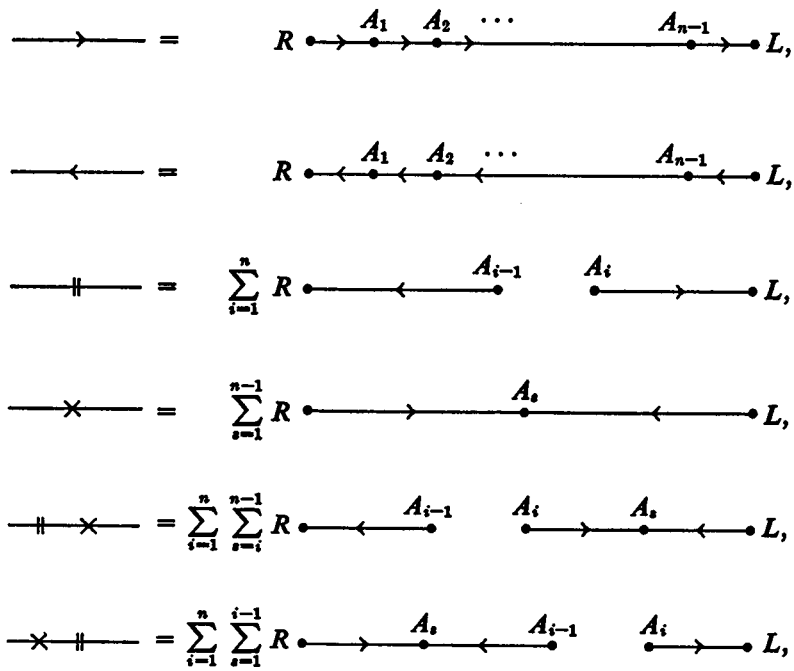

(18)

which applies analogously to the type 2 branch. On the right-hand sides of Eq. 18 the directed lines represent products of the corresponding rate constants.

The evaluation of Eqs. 17 and 18 is tedious, but not at all difficult. The algebraic result reads

$$S = k_1^n k_2^{n-1} \sigma_{12} + k_2^n k_1^{n-1} \sigma_{21}, \tag{19}$$

$$\sigma_{12} = [c_1 e^{nx_1} + c_1' e^{-nx_1} + c_1 c_1' g(x_1)] f(x_2) + c_1 c_2' e^{nx_1} h(-x_2) + c_1' c_2 e^{-nx_1} h(x_2), \tag{20}$$

$$\left.\begin{aligned} f(x) &= \frac{\sinh (nx)}{\sinh x}, \qquad g(x) = \frac{\sinh [(n-1)x]}{\sinh x} \\ h(x) &= \frac{1}{2 \sinh x}\left[(n-1)e^{nx} - \frac{\sinh [(n-1)x]}{\sinh x}\right] \end{aligned}\right\}, \tag{21}$$

σ_{21} is easily obtained from Eq. 20 by permutation of 1, 2.

In order to express the steady-state flux, we still have to construct the flux diagrams as required by the above theorem. In general, a particular diagram for the steady-state flux along a certain line is obtained from the original diagram by omitting the minimum possible number of lines such that the resulting diagram retains exactly one cycle which contains the considered line as a part. All noncyclic lines are directed into the cycle, and the algebraic value of the cycle itself is the difference of the rate constant products for its two possible orientations. Again, the sum of all flux diagrams along a line is the sum over all ways of forming particular flux diagrams along this line.

In our case, the structure of the original diagram Eq. 15 is very simple, and all possible flux diagrams topologically coincide with the original diagram. The sum over all flux diagrams for the steady-state flux of ions of type 1 along any of their transition lines is thus given by

$F_1 =$ 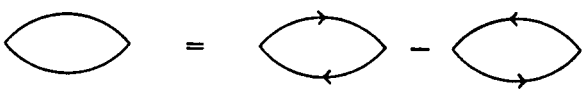 (22)

$$= (k_1 k_2)^n [c_1 c_2' e^{n(x_1 - x_2)} - c_1' c_2 e^{-n(x_1 - x_2)}].$$

Clearly, the corresponding expression for the ions of type 2 is

$$F_2 = -F_1. \tag{23}$$

Finally, the steady-state flux per chain of the ions of type 1 is given by

$$j_1 = \frac{F_1}{S} = k_1 \frac{c_1 c_2' e^{n(x_1 - x_2)} - c_1' c_2 e^{-n(x_1 - x_2)}}{\frac{k_1}{k_2} \sigma_{12} + \sigma_{21}}, \tag{24}$$

and $j_2 = -j_1$.

b. Three-Channel Model

In the same way we shall now examine the case where only one type of ion (say, of type 2) can pass the chain and rearrangement of the chain's polarization is due to

the passage of the two possible kinds of bonding defects (denoted by the subscripts 3 and 4 as given in Eqs. 3 *a* and 3 *b*).

This version of the model applies to all cases where w and $\epsilon_2 = \epsilon_{DC}^{(2)} - \epsilon_s^{(2)}$ are of the same order of magnitude, but

$$\epsilon_i \gg \epsilon_2 \quad \text{for all} \quad i \neq 2. \tag{25}$$

States with one ion and one bonding defect simultaneously present in the chain have an energy $\epsilon_2 + w$ compared with that of the ground state without ion and without bonding defect. Neglecting the states with energies $\epsilon_2 + w$ while including the states with one ion or one bonding defect is consistent only if

$$e^{-w/k_BT} \ll 1, \qquad e^{-\epsilon_2/k_BT} \ll 1. \tag{26}$$

Since we now have a three-channel mechanism, our basic diagram is given by

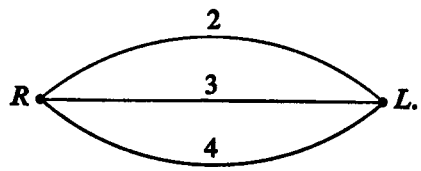

(27)

The sum S of all directed partial diagrams is obtained as

$$S = S_{234} + S_{342} + S_{423}, \tag{28}$$

where

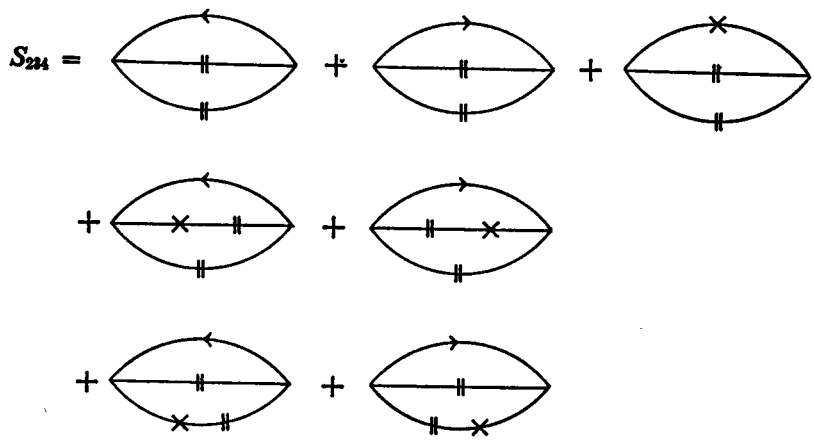

(29)

$$= k_2^n (k_3 k_4)^{n-1} \sigma_{234},$$

$$\begin{aligned}\sigma_{234} = {} & [c_2 e^{nx_2} + c_2' e^{-nx_2} + c_2 c_2' g(x_2)] f(x_3) f(x_4) \\ & + [c_2 c_3' e^{nx_2} h(-x_3) + c_2' c_3 e^{-nx_2} h(x_3)] f(x_4) \\ & + [c_2 c_4' e^{nx_2} h(-x_4) + c_2' c_4 e^{-nx_2} h(x_4)] f(x_3).\end{aligned} \tag{30}$$

Eq. 30 still contains the general case that each of the three channels 2, 3, 4 in Eq. 27 belongs to a different ion. In our special case where 3 and 4 are bonding defects with zero valencies $\nu_3 = \nu_4 = 0$ we have

$$x_3 = x_4 = -2\alpha\varphi, \qquad \varphi = \frac{eU}{2nk_BT}, \tag{31}$$

$$k_3 = k_4 = k, \tag{32}$$

where k is the rate constant for the reversal of a dipole without ionic transition. For the effective concentrations c_3, c_3', c_4, c_4' of the bonding defects it is necessary to insert

$$c_3 = c_3' = c_4 = c_4' = r = \exp\left(-\frac{w}{k_BT}\right), \tag{33}$$

since the free concentration of bonding defects is unity and w, the formation energy of a bonding defect, describes an effective repulsion energy between the defect and the membrane. S_{342}, S_{423} and σ_{342}, σ_{423} can be derived from Eqs. 29 and 30 by cyclic permutation of the indices; it is readily shown that in our special case $\sigma_{342} = \sigma_{423}$.

For the steady-state flux diagrams of the type 2 ions in a three-channel model we now have two options:

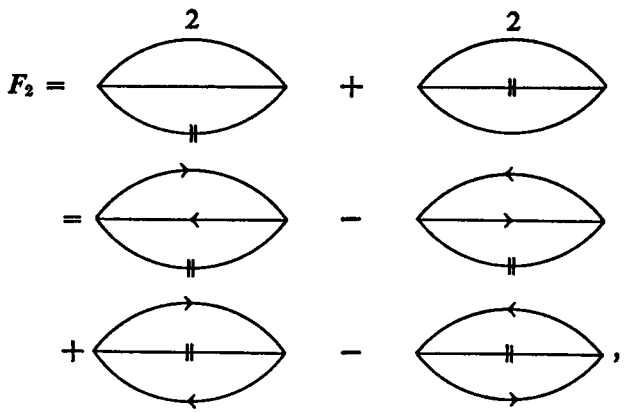

(34)

$$= (k_2 k_3)^n k_4^{n-1}[c_2 c_3' e^{n(x_2-x_3)} - c_2' c_3 e^{-n(x_2-x_3)}] f(x_4)$$
$$+ (k_2 k_4)^n k_3^{n-1}[c_2 c_4' e^{n(x_2-x_4)} - c_2' c_4 e^{-n(x_2-x_4)}] f(x_3),$$
$$= 2k_2^n k^{2n-1} r[c_2 e^{n\nu_2\varphi} - c_2' e^{-n\nu_2\varphi}] f(-2\alpha\varphi).$$

Combining Eqs. 29, 30, and 34, the steady-state flux of type 2 ions per chain in our special model finally is found to be

$$j_2 = \frac{F_2}{S} = 2k_2 r \frac{c_2 e^{n\nu_2\varphi} - c_2' e^{-n\nu_2\varphi}}{\frac{k_2}{k}\sigma_{234} + 2\sigma_{342}} \cdot f(-2\alpha\varphi). \tag{35}$$

4. DISCUSSION OF RESULTS

Asymptotic Evaluation and Instabilities

Although we have obtained analytic expressions for our steady-state fluxes, Eqs. 24 and 35, we cannot immediately discuss the fluxes as a function of voltage and concentration since our results are rather intricate. On the other hand a discussion of the asymptotic properties of our results for small and large values of concentrations and voltages does not present any difficulties. Let us start by considering the steady-state fluxes as a function of the concentrations.

a. Dependence on Concentration

Let us discuss j_1 as a function of c_1, the concentration of type 1 ions on the left side of the membrane, while c_1', c_2, c_2', and the voltage remain constant. From Eq. 20 we conclude that the denominator in Eq. 24 is finite for $c_1 = 0$ and increases linearly with increasing c_1. If the second-order terms in the concentrations are assumed to be small compared with the first-order terms, we expect

$$\frac{k_1}{k_2}\sigma_{12} + \sigma_{21} \rightarrow \begin{cases} \dfrac{k_1}{k_2} c_1' e^{-nx_1} + c_2 e^{nx_2} + c_2' e^{-nx_2} & c_1 \rightarrow 0, \\ \dfrac{k_1}{k_2} c_1 e^{nx_1} & c_1 \rightarrow \infty. \end{cases} \tag{36}$$

Since the denominator of Eq. 24 is also a linear function of c_1 and has a finite negative value for $c_1 = 0$ (if $c_1' \neq 0$), we expect j_1 to increase linearly with c_1 for small c_1 and to show saturation at high c_1 as indicated in Fig. 4.

From Eq. 36 we conclude that the c_1 range in which saturation becomes observable depends on the values of c_1', c_2, c_2', U, and k_1/k_2, but may well be within experimentally reasonable or even low orders of magnitude.

By permutation of 1, 2 we can easily extend our discussion to include j_1 as a function of c_2. If we put $c_1 = c_1'$, the denominator of Eq. 24 becomes a quadratic func-

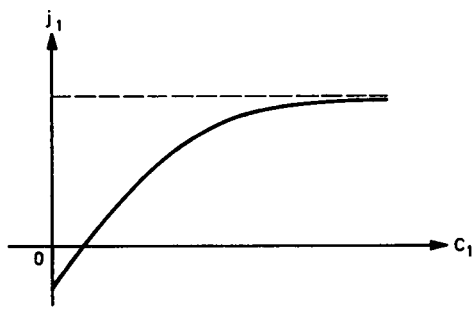

FIGURE 4 Expected dependence of j_1 on c_1 at constant c_1', c_2, c_2', U in the two-channel model.

tion of c_1. This implies a linear increase of j_1 with c_1 at low values of c_1 and a decrease $\sim 1/c_1$ at high values so that $j_1(c_1)$ must have a maximum at medium values of c_1. The decrease of j_1 at very high c_1 is due to the fact that the probability for a type 1 ion to be present in the chain increases at the expense of the probability of a type 2 ion to be present to such an extent that eventually the chain can no longer rearrange itself and thus fails to be permeable for any ion.

Essentially the same discussion as above applies to the three-channel model: again the denominator of Eq. 35 is a linear function of c_2 so that $j_2(c_2)$ increases linearly with c_2 at low values of c_2 and shows saturation at high values of c_2.

b. High Voltage Behavior

Let us now turn to the fluxes as a function of the applied voltage U. From Eqs. 24 and 35 one can easily calculate the ionic conductivity of a chain in the linear $j - U$ range. Of greater interest and importance is the behavior of the fluxes for very high values of the applied voltage U. Let us therefore evaluate the denominators of Eqs. 24 and 35 asymptotically for $U \to \infty$.

Since

$$x_i = (\nu_i - 2\alpha)\frac{eU}{2nk_BT},$$

we have

$$\lim_{U\to\infty} x_1 = +\infty \quad \text{if} \quad 0 \leq \alpha \leq 1,$$

$$\lim_{U\to\infty} x_2 = \begin{cases} +\infty & \text{if} \quad 0 \leq \alpha < \frac{1}{2} \\ -\infty & \text{if} \quad \frac{1}{2} < \alpha \leq 1. \end{cases} \tag{37}$$

It is easily verified that for $U \to \infty$ the leading terms in the denominator of Eq. 24 are

$$\frac{k_1}{k_2}\sigma_{12} + \sigma_{21} \to \begin{cases} \sim \exp\{[3n - 1 - 2\alpha(2n-1)]\varphi\} & 0 \leq \alpha < \frac{1}{2} \\ \sim \exp\{[n + 1 - 2\alpha]\varphi\} & \frac{1}{2} < \alpha < \frac{3}{4} \\ \sim \exp\{[n - 2 + 2\alpha]\varphi\} & \frac{3}{4} < \alpha \leq 1, \end{cases}$$

$$\varphi = \frac{eU}{2nk_BT}. \tag{38}$$

The numerator of Eq. 24 for $U \to \infty$ is written

$$c_1 c_2' e^{n(x_1-x_2)} - c_1' c_2 e^{-n(x_1-x_2)} \to \sim e^{n\varphi}. \tag{39}$$

From Eqs. 38 and 39 we immediately conclude that

$$\lim_{U\to\infty} j_1 = \begin{cases} 0, & 0 \le \alpha < \frac{1}{2} \\ \infty, & \frac{1}{2} < \alpha \le 1. \end{cases} \tag{40}$$

We therefore expect a flux-voltage curve of the type roughly sketched in Fig. 5, i.e., $j_1(U)$ shows a maximum at some $U = U_s$ for $0 \le \alpha < \frac{1}{2}$.

In the three-channel model, $\nu_2 > 0$, $\nu_3 = \nu_4 = 0$, we have

$$\left.\begin{aligned} \lim_{U\to\infty} x_2 &= \begin{cases} +\infty, & 0 \le \alpha < \frac{1}{2} \\ -\infty, & \frac{1}{2} < \alpha \end{cases} \\ \lim_{U\to\infty} x_3 &= \lim_{U\to\infty} x_4 = -\infty. \end{aligned}\right\} \tag{41}$$

The asymptotic values of the denominator and the numerator of Eq. 35 for $U \to \infty$ are

$$\frac{k_2}{k}\sigma_{234} + 2\sigma_{342} \to \begin{cases} \sim \exp\{[n\nu_2 + 2\alpha(n-2)]\varphi\} & 0 < \alpha < \frac{\nu_2}{4} \\ \sim \exp\{[(n-1)\nu_2 + 2\alpha n]\varphi\} & \frac{\nu_2}{4} < \alpha < \frac{\nu_2}{2} \\ \sim \exp\{[2\alpha(3n-2) - (n-1)\nu_2]\varphi\} & \frac{\nu_2}{2} < \alpha \end{cases} \tag{42}$$

$$(c_2 e^{n\nu_2\varphi} - c_2' e^{-n\nu_2\varphi}) f(-2\alpha\varphi) \to \sim \exp\{[n\nu_2 + 2\alpha(n-1)]\varphi\}, \tag{43}$$

so that

$$\lim_{U\to\infty} j_2 = \begin{cases} \infty, & 0 \le \alpha < \frac{\nu_2}{2} \\ 0, & \frac{\nu_2}{2} < \alpha. \end{cases} \tag{44}$$

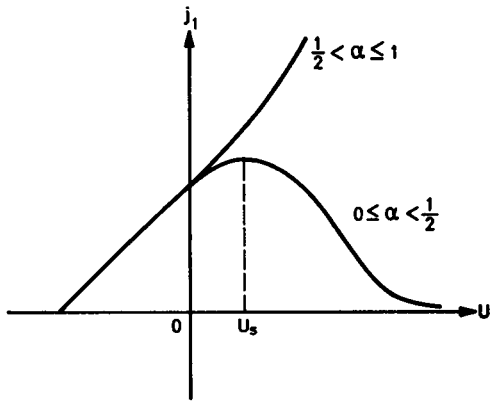

FIGURE 5 Expected flux-voltage curve for the two-channel model.

When comparing Eq. 40 with Eq. 44 we note that the asymptotic behavior of j_1 for $U \to \infty$ in the two-channel model with $\nu_1 = 2$, $\nu_2 = 1$ and that of j_2 in the three-channel model with $\nu_2 = 1$, $\nu_3 = \nu_4 = 0$ (bonding defects) are complementary.

c. Physical Interpretation of the High Voltage Results

The results 40 and 44 can be interpreted by means of a simple physical argument. In the two versions of the model the complete transport cycle consists of two phases: for example, in the two-channel model passage of a type 1 ion from R to L and passage of a type 2 ion from L to R

$$R \xrightarrow{1} L \xrightarrow{2} R. \tag{45}$$

Each phase involves a change in electrostatic energy as follows

$$\left.\begin{aligned} \Delta E(R \to L) &= -eU(\nu_1 - 2\alpha) \\ \Delta E(L \to R) &= eU(\nu_2 - 2\alpha) \end{aligned}\right\}, \tag{46}$$

such that

$$-[\Delta E(R \to L) + \Delta E(L \to R)] = eU(\nu_1 - \nu_2) = T\Delta S_i \geq 0, \tag{47}$$

where ΔS_i is the internal production of entropy in the course of the complete cycle. The second law of thermodynamics requires that expression 47 is nonnegative: at $U > 0$ type 1 ion will pass from R to L and type 2 ion will pass from L to R if $\nu_1 > \nu_2$ and vice versa. This implies that the sum of the two expressions in Eq. 46 is negative, whereas it does not require that each term is negative. For example, if $\nu_2 = 1$ and $0 < \alpha < \frac{1}{2}$, $\Delta E(L \to R) > 0$, there is a decrease in electrostatic energy in the first phase of the cycle and an increase in the second. Therefore, the intermediate

state L has the lowest electrostatic energy and may be considered to act as a "trap" for the ionic flux. At $U \to \infty$ the depth of the trap becomes infinitely large and hence the flux tends to zero. A similar argument applies to the three-channel model with $\alpha > \nu_2/2$; in this case, the intermediate state acts as a barrier.

d. Four-Channel Model

Combination of the two-channel and the three-channel versions of the dipole chain model leads to a four-channel model describing the passage of two types of cations with $\nu_1 = 2$, $\nu_2 = 1$ and, in addition, the passage of the two types of bonding defects $\nu_3 = \nu_4 = 0$. The basic diagram is then given by

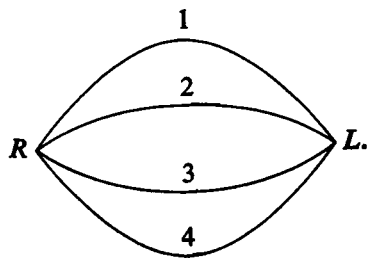

(48)

The sum S of all directed partial diagrams in this case is easily derived from Eqs. 28–30 by consequent generalization. The flux diagrams of the cations of type 1 and 2 result to be

$$F_i = F_i' + F_i'', \quad i = 1, 2, \tag{49}$$

$F_1' =$ 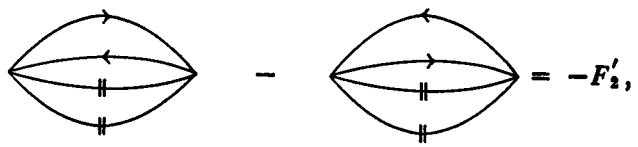 $= -F_2'$, (50)

$F_1'' =$ 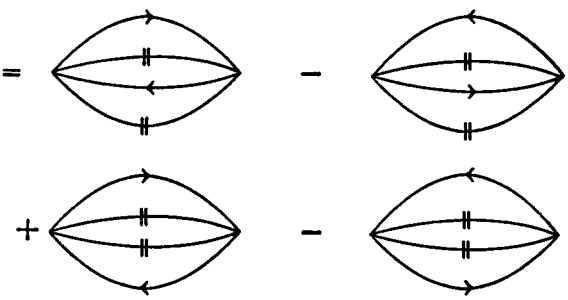 , (51)

and likewise for F_2'' (numbering of the channels as in Eq. 48). Correspondingly we define the various fluxes as

$$j_i = \frac{F_i}{S}, \quad j_i' = \frac{F_i'}{S}, \quad j_i'' = \frac{F_i''}{S}. \tag{52}$$

j_1' is that part of the 1 flux which is associated with an opposite flux of type 2 and vice versa, whereas j_i'' is the flux contribution of type i associated with the passage of a bonding defect of any type. For the net flux of electric charge per chain we obtain

$$j_e = e(2j_1 + j_2). \tag{53}$$

Let us now discuss the behavior of j_e as a function of the voltage U for $0 \leq \alpha < \frac{1}{2}$. If $\epsilon_i < w$ (ϵ_i as defined in Eq. 13 and w denoting the formation energy of a bonding defect), and ϵ_1 and ϵ_2 are of the same order of magnitude, at low voltages U we expect a behavior very similar to that of the two-channel model, i.e., channels 3 and 4 of the bonding defects are closed:

$$\left.\begin{aligned} &j_i'' \approx 0, \quad i = 1, 2 \\ &j_1 \approx j_1' = -j_2' \approx -j_2 \\ &j_e \approx e j_1' \end{aligned}\right\} \text{ small } U\text{'s}. \tag{54}$$

The charge flux in this region is almost completely due to an antiparallel flux of the ions of types 1 and 2. For increasing values of U, the passage of bonding defects becomes more and more likely, whereas the antiparallel flux of two positive ions is increasingly unfavorable since $0 \leq \alpha < \frac{1}{2}$, compare Eq. 40. Eventually, the antiparallel flux of ions 1 and 2 vanishes, the net charge transfer is almost completely due to a parallel ionic flux, and rearrangement of the chain is achieved by passage of bonding defects:

$$\left.\begin{aligned} &j_i' \approx 0, \quad i = 1, 2 \\ &j_1 \approx j_1'', \quad j_2 \approx j_2'' \\ &j_e \approx e(2j_1'' + j_2'') \end{aligned}\right\} U \to \infty. \tag{55}$$

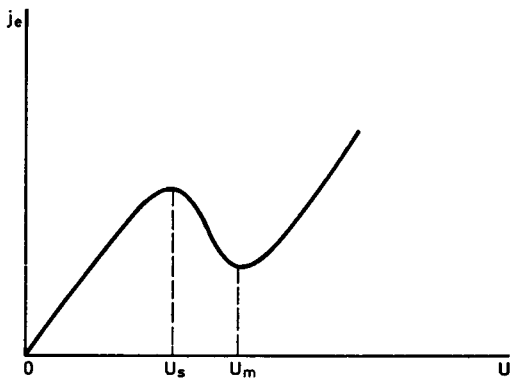

FIGURE 6 Expected curve of the net flux j_e of electric charge as a function of voltage U in the four-channel model.

If the differences $w - \epsilon_i$, $i = 1, 2$ are sufficiently large, the net charge flux j_e of the four-channel model as a function of U will follow the corresponding curve of the two-channel model for increasing U up to negative values of dj_e/dU, i.e., even including the maximum of j_e at $U = U_s$. Owing to the opening of the bonding defect channels at very high U, however, the net charge flux will again increase with U so that the maximum at U_s is followed by a minimum of j_e at $U = U_m$, as shown in Fig. 6. The numerical evaluation of our model in section 5 will confirm this qualitative conclusion.

e. Instabilities: Electrical Excitation

From the thermodynamic point of view, the existence of a maximum of the net charge flux $j_e(U)$ as a function of voltage U

$$\left(\frac{dje}{dU}\right)_{U=U_s} = 0, \tag{56}$$

entails a physical instability. In our previous considerations, we have shown that for $0 \leq \alpha < \frac{1}{2}$ such a maximum necessarily exists in the two-channel model and upon appropriate choice of the parameters w, ϵ_i, in the four-channel model as well. From the biophysical viewpoint, an instability of this type is of major interest as it represents a possible mechanism for electric excitation of the membrane. For current-voltage characteristics like that shown in Fig. 5 (for $0 \leq \alpha < \frac{1}{2}$) and that in Fig. 6 it is always possible to construct a load line of an appropriate external circuit in such a way that it intersects the characteristic in three different points, the operating points of the complete circuit (see Fig. 7). As shown by Franck and Kettner [6–8], only the outer two operating points (U_1 and U_3 in Fig. 7) are stable whereas the inner one (U_2) is metastable so that the complete system runs into U_1 if the instantaneous value of the voltage U is smaller than U_2 or into U_3 if U is greater than

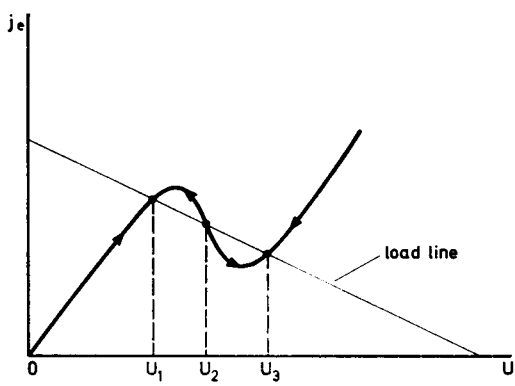

FIGURE 7 Bistability in the four-channel model.

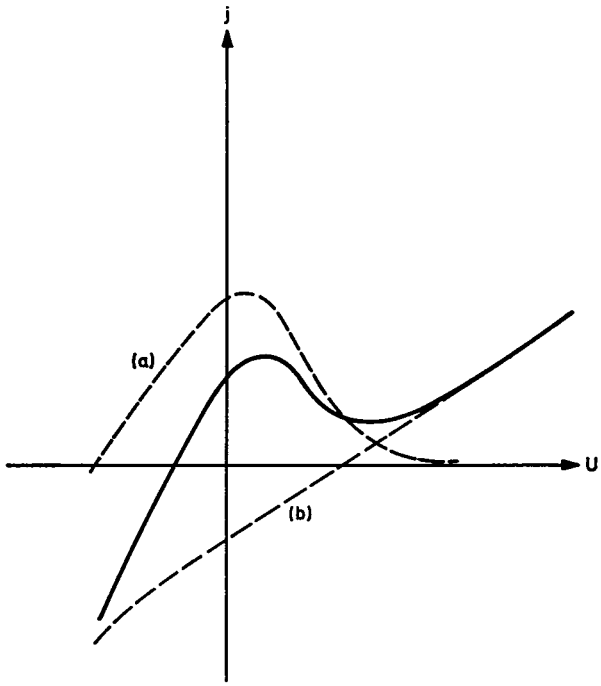

FIGURE 8 Superposition of a two-channel chain (*a*) and a three-channel chain (*b*). The solid curve shows the total flux.

U_2. This bistability of the complete system is a possible model for membrane excitation, for example, in nerves.

N-shaped flux-voltage curves (i.e., voltage-controlled instabilities) can also be obtained by a superposition of two different dipole chains. To give an appropriate example, let us assume that one of the chains is of the kind of our two-channel model for antiparallel flux of a bivalent (type 1, for example Ca^{2+}) and a monovalent (type 2, for example Na^+) ion, whereas the other chain is of the kind of our three-channel model for the same monovalent (type 2) ion and bonding defects. For both chains we assume $0 \leq \alpha < \frac{1}{2}$. If now the concentrations satisfy the conditions

$$c_1 > c_1', \quad c_2 < c_2',$$

(for example surplus Ca^{2+} outside and Na^+ inside) the separate flux-voltage curves for the two chains may look like the dotted lines in Fig. 8. The total flux again is N-shaped as in Fig. 7.

5. NUMERICAL EVALUATION

Our qualitative results in the previous section are easily confirmed by a computer evaluation of Eqs. 24 and 35. Fig. 9 shows computed curves of the flux-voltage

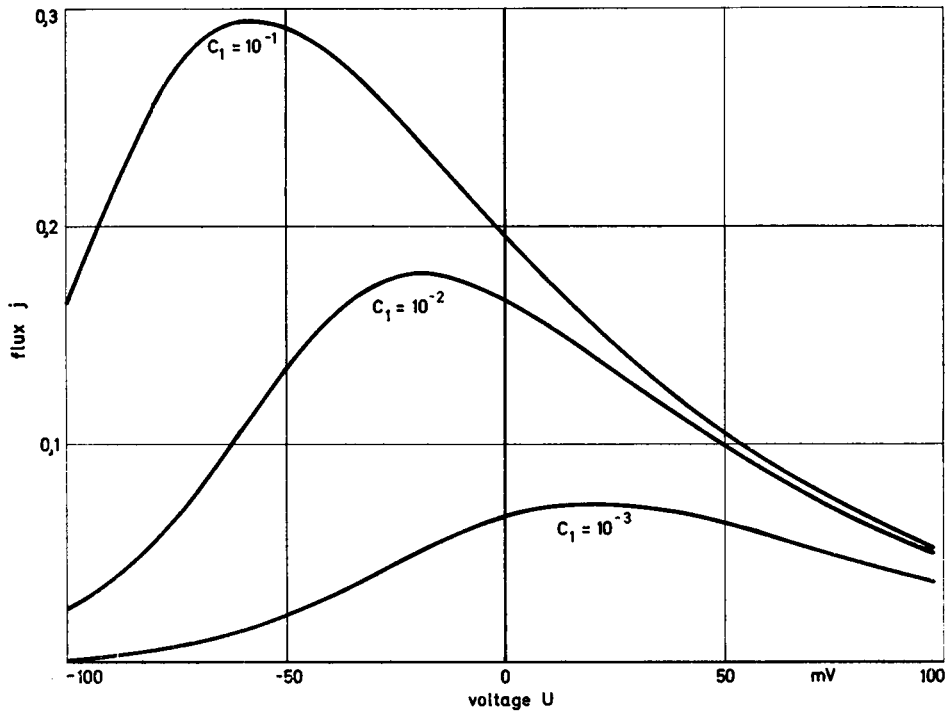

FIGURE 9 Computed flux-voltage curve for the two-channel model at different c_1 values ($c_1' = 0$, $c_2 = c_2' = 10^{-3}$, $\alpha = 0.2$, $n = 5$, $k_1/k = k_3/k = 1$).

characteristic for the two-channel model ($\alpha = 0.2$; number of dipoles equals $n = 5$).

For biophysical applications it is interesting to investigate the variation of the threshold voltage U_s as a function of the internal effective concentration c_1 of the bivalent ions. Usually, this relation is referred to as

$$\Gamma = \frac{dU_s}{d \ln c_1}. \tag{57}$$

Fig. 10 shows computed curves of U_s as a function of $\ln c_1$ in the two-channel model for different values of $\alpha (0 \leq \alpha < \frac{1}{2})$. From these curves we see that

$$\Gamma \to 0 \quad \text{for} \quad c_1 \to \pm\infty. \tag{58}$$

There is an intermediate region, however, where Γ is almost constant:

$$\left.\begin{aligned} \Gamma &= \Gamma_{max} < 0 \\ U_s &= -|\Gamma_{max}| \cdot \ln c_1 \end{aligned}\right\}, \tag{59}$$

A further numerical analysis shows that $|\Gamma_{max}|$ only depends on α, and not on

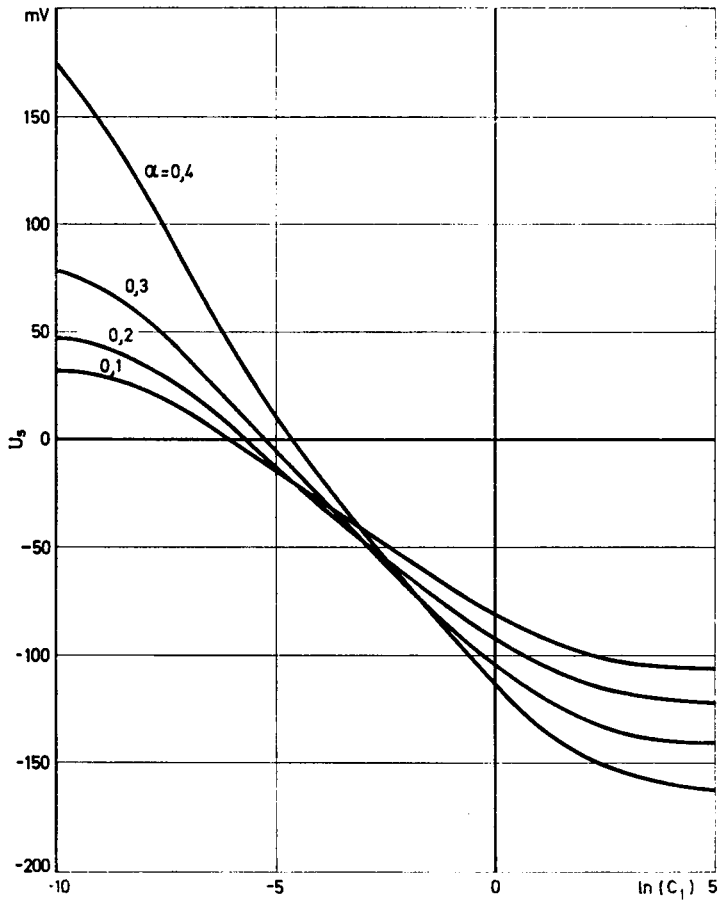

FIGURE 10 Computed threshold voltage U_s as a function of ln c_1 in the two-channel model for different values of $\alpha(c_1' = 0, c_2 = c_2' = 10^{-3}, n = 5, k_1/k = k_2/k = 1)$.

the other parameters like n, k_1/k, k_2/k, c_2, c_2'. (k_1, k_2, k are the voltage-free rate constants of the ions of type 1, 2 and of the bonding defects.) In Fig. 11 $|\Gamma_{max}|$ is plotted as a function of $(\frac{1}{2} - \alpha)^{-1}$, which is approximately a linear relationship. Moreover, we see that

$$|\Gamma_{max}| \geq \frac{kT}{2e} = 12,9 \text{ mV (for } T = 300^\circ \text{ K}). \qquad (60)$$

Experimentally, electrical excitation and the existence of a threshold voltage like that in our two-channel model have been found in membranes of nerves (9) and of amphibian epithelia (10). The experimental Γ values range between -9 and -6 mV for nerve and ≈ -18 mV for amphibian epithelia, respectively. The latter value

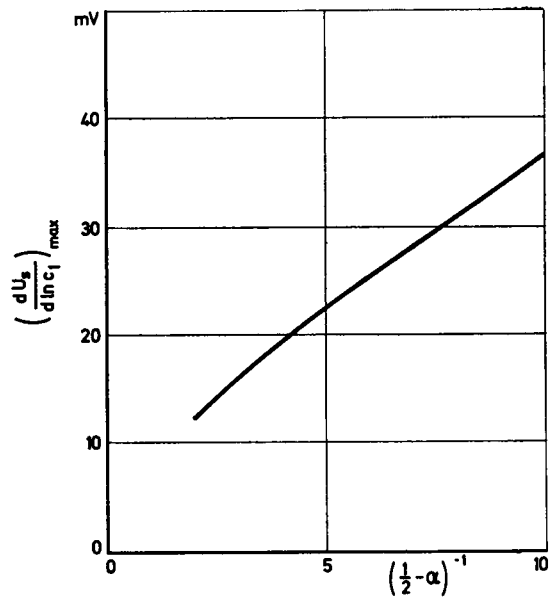

FIGURE 11 Computed maxima of $dU_s/d(\ln c_1)$ as a function of $(\frac{1}{2} - \alpha)^{-1}$ in the two-channel model ($c_1' = 0$, $c_2 = c_2' = 10^{-3}$, $n = 5$, $k_1/k = k_2/k = 1$).

is within the range of $|\Gamma_{max}|$, Eq. 60, whereas for nerve we would have to refer to the transition regions between $\Gamma \approx 0$ and $\Gamma = \Gamma_{max}$ in our model.

We also tried to obtain numerically an N-shaped flux-voltage curve from the four-channel version of our model as described in section 4 *d*. By giving the energy w of bonding defects a sufficiently large value we can actually arrive at a very pronounced N-shape. It turns out, however, that this is possible only at the expense of the values for U_s and U_m, i.e., the voltages at which the flux has its maximum and minimum, increasing by up to several 100 mV; this is far beyond any biophysically reasonable voltage range. The more pronounced the N,-shape, i.e., the larger

$$\frac{\Delta j}{j} = \frac{j_{max} - j_{min}}{j_{max}}, \qquad (61)$$

the larger are necessarily the values of U_s and U_m. This fact is consistent with our intuitive understanding of the four-channel model. In order to find the optimum within these limitations we have developed a feedback computer routine in which all parameters are systematically varied and a particular variation step is repeated if its effect was favorable or canceled if it was unfavorable. Beginning this routine with different initial values of the parameters we always arrived at the same optimum within a matter of a few minutes of computing time. As the lower limit for $\Delta j/j$, Eq. 61, we imposed $\Delta j/j \geq 0.2$. The result of this procedure is shown in Fig. 12.

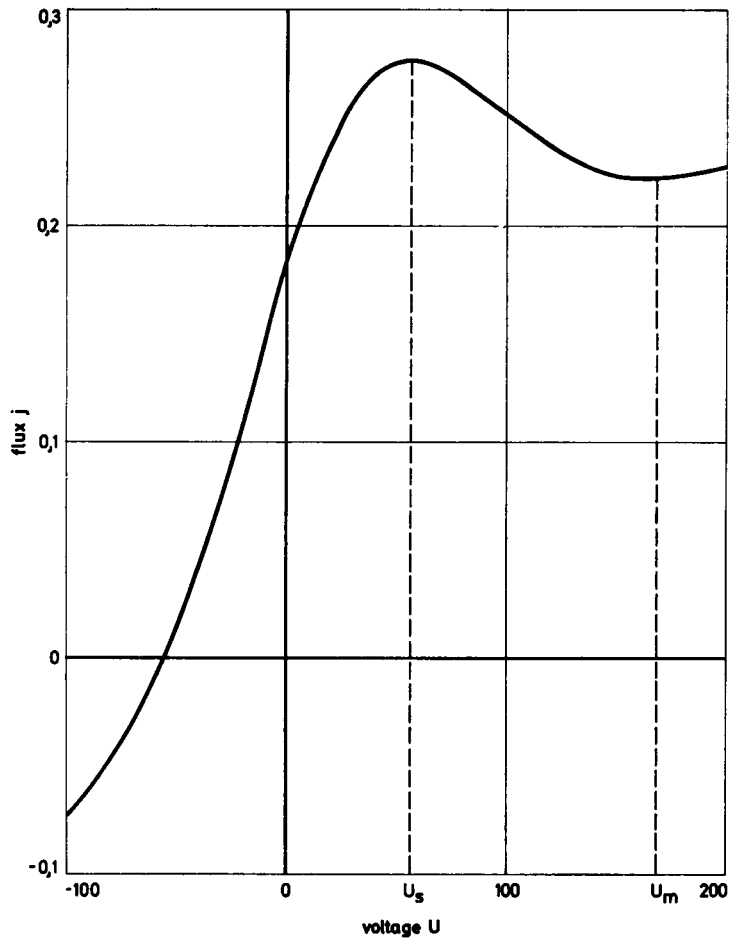

FIGURE 12 Computed flux-voltage curve of optimum N-shape in the four-channel model; $c_1 = 10^{-3}$, $c_1' = 0$, $c_2 = 2 \times 10^{-3}$, $c_2' = 10^{-3}$, $\alpha = 0.2$, $n = 4$, $r = \exp(-w/k_BT) = 10^{-7}$, $k_1/k = 2 \times 10^{-3}$, $k_2/k = 2.5 \times 10^{-2}$.

6. CONCLUDING REMARKS

Although Onsager's model is so attractive because of its very simple structure and the small number of additional assumptions made, one may still raise the standard objection which is often raised to theoretical models: if the number of the adjustable parameters is large enough, every model can be forced to describe every experiment with sufficient accuracy.

We feel, however, that in this case the situation is somewhat different. First of all, the number of parameters is not so large. The parameters which have to be adjusted are α, n, w, k_1/k_2 (or k_1/k, k_2/k) in addition to two further factors describing the

ratio of the effective and true concentrations of the ions of types 1 and 2. Secondly, Onsager's model claims a molecular mechanism. This means that almost all parameters bear a defined physical meaning on a molecular scale. Therefore, it should be possible at least to narrow down the range in which the parameters can be adjusted by estimating their order of magnitude. The third point is that the numerical evaluation particularly of the four-channel model in section 5 has shown us that the model is not very flexible. In fact, we have not been able to reproduce every kind of an N-shaped characteristic that we wanted.

From these considerations we conclude that it will not be very difficult to put the whole model to a crucial test by comparing the predicted results with experimental findings which either have been obtained by other researchers or could readily be obtained in the future.

The author would like to thank Professor Dr. Klaus Heckmann (Universität Regensburg, West Germany) and Professor Dr. Bernd Lindemann (Universität des Saarlandes, West Germany) for many helpful and stimulating discussions.

The author is also very much indebted to Professor Dr. Hans Neurath (University of Washington, Seattle, Washington, and Battelle Seattle Research Center) who generously supported this work under the Life Sciences Program of Battelle Memorial Institute.

Received for publication 15 June 1972.

REFERENCES

1. ONSAGER, L. 1970. *In* Physical Principles of Biological Membranes. F. Snell, J. Wolken, G. J. Iverson, J. Lam, editors. Gordon and Breach Science Publishers, Inc., New York. 137.
2. HILL, T. L. 1966. *J. Theor. Biol.* **10**:442.
3. KIRCHHOFF, G. 1847. *Poggendorffs Ann. Phys. Chem.* **72**:495.
4. BOTT, R., and J. P. MAYBERRY. 1954. *In* Matrices and Trees, Economic Activity Analysis J. Wiley and Sons, Inc., New York. 391.
5. KING, E. L., and C. ALTMANN. 1956. *J. Phys. Chem.* **60**:1375.
6. FRANCK, U. F., and F. KETTNER. 1964. *Ber. Bunsenges. Phys. Chem.* **68**:875.
7. FRANCK, U. F. 1965. *Stud. Gen. (Z. Interdisziplinaere Stud.).* **18**:313.
8. FRANCK, U. F. 1967. *Ber. Bunsenges. Phys. Chem.* **71**:789.
9. FRANKENHAEUSER, B., and A. L. HODGKIN. 1957. *J. Physiol. (Lond.).* **137**:218.
0. LINDEMANN, B. 1968. *Biochem. Biophys. Acta.* **163**:424.